

Vortex Structure and Critical Currents in Josephson Junctions*

C. S. OWEN AND D. J. SCALAPINO†

*Department of Physics and Laboratory for Research on the Structure of Matter,
University of Pennsylvania, Philadelphia, Pennsylvania*

(Received 26 May 1967)

The maximum current that can be carried by a long unbiased superconducting tunnel junction as a function of applied magnetic field has been calculated. A symmetric junction geometry was assumed for which the boundary conditions relate the space derivatives of the phase difference ϕ at the two ends. In addition, we graph the current density distribution within the junction when the total current is maximum, and we show the shape of the current vortices in the large-field case and the details of the self-limiting of the tunnel current as a function of junction length in zero applied field.

I. INTRODUCTION

EVIDENCE that a weak magnetic field could modulate the current carried by a superconducting tunnel junction provided striking confirmation of the Josephson dc effect.^{1,2} For a uniform junction of small dimension or low critical current, the magnetic field due to the tunneling current can be neglected. In this case, the maximum current variation with applied magnetic field follows a Fraunhofer diffraction pattern.^{2,3} As the junction size or critical current increases, the influence of the current-induced magnetic field becomes important. Below a critical field, a semi-infinite junction exhibited a Meissner effect, screening the external field at the Josephson penetration distance λ_J .⁴ The importance of the tunneling-current-induced field is measured by the ratio of λ_J to the dimension L of the junction perpendicular to the external field. Here we will discuss the dependence of the junction critical current on magnetic field and on the ratio L/λ_J . The detailed spatial structure of the current density and magnetic field will also be shown.

In Sec. II, the junction geometry and the basic equations which describe the Josephson tunneling phenomena are briefly reviewed. The equations have been derived by a number of people.⁵ Anderson in particular has used these equations to discuss the single vortex and *Abrikosov array* of quantized vortices which can exist in a junction. The equations are solved in terms of elliptic functions, and the boundary conditions are satisfied by a graphical method.

Results from this analysis are plotted and discussed in Sec. III. The major result is a plot of the junction critical current versus magnetic field for a junction with

an L/λ_J ratio of 10. This illustrates the interesting features which are present for a large L/λ_J ratio. We find that for a given magnetic field, there may be several allowed current distributions differing in the number of vortices they contain. Each of these solutions has its own critical current. The junction critical current presumably switches to that mode which is capable of carrying the maximum critical current for a given value of H . The current density and field distributions in the junction are shown for a number of special cases.

II. BASIC EQUATIONS

The geometry of the junction is shown in Fig. 1. Theoretically it consists of two semi-infinite superconducting sheets which overlap for a distance L in the z direction. In the overlap region the superconductors are separated by a thin insulating layer. We imagine that the current flows in at the left from $z = -\infty$ and out at the right toward $z = \infty$. The tunneling probability peaks sharply in the direction perpendicular to the junction interface, so that the important tunneling current density is along the x direction. The modifications of this which occur at the edge of the junction are on the scale of the London penetration depth, which is completely negligible for this analysis which is concerned with variations on the scale of the Josephson penetration depth.

Because of the symmetry of this configuration, the variables can only depend upon the z coordinate. Experimentally, a junction geometry approaching our idealized form can be obtained by making the y dimension *either* large or small compared to λ_J . If it is small and the external field is along the y axis, there is no way for spatial variations to be generated in the y direction.

Josephson showed that the current density was given in terms of the relative pair phase $\phi(z)$ across the insulator by

$$j(z) = j_1 \sin \phi(z). \quad (1)$$

Furthermore, the gradient of the phase is proportional-

* Supported in part by the National Science Foundation and the Advanced Research Projects Agency.

† Alfred P. Sloan Foundation Fellow.

¹ P. W. Anderson and J. M. Rowell, *Phys. Rev. Letters* **10**, 230 (1963).

² J. M. Rowell, *Phys. Rev. Letters* **11**, 200 (1963).

³ M. D. Fiske and I. Giaever, *Proc. IEEE* **52**, 1155 (1964).

⁴ R. A. Ferrell and R. E. Prange, *Phys. Rev. Letters* **10**, 479 (1963); B. D. Josephson, *Advan. Phys.* **14**, 419 (1965).

⁵ B. D. Josephson, *Advan. Phys.* **14**, 419 (1965); P. W. Anderson (to be published); Y. M. Ivanchenko, A. V. Svidzinski, and V. A. Slusarev, *Zh. Eksperim. i Teor. Fiz.* **51**, 194 (1966) [English transl.: *Soviet Phys.—JETP* **24**, 131 (1967)].

to the local field

$$\partial\phi/\partial z = (2ed/\hbar c)H(z). \quad (2)$$

Here d is equal to twice the penetration depth (for identical superconductors) plus the insulator thickness. Combining (1) and (2) with the Maxwell equation

$$(\partial^2/\partial z^2)H(z) = (4\pi/c)j(z), \quad (3)$$

one obtains a differential equation which determines ϕ in the absence of a voltage bias,

$$(\partial^2/\partial z^2)\phi = (1/\lambda_J^2) \sin\phi. \quad (4)$$

Here, $\lambda_J = [\hbar c^2/8\pi e d j_1]^{1/2}$ is the Josephson penetration depth.

We are interested in the case in which there is an applied external magnetic field H_e and a current

$$I = \int_0^L j(z) dz \quad (5)$$

flowing per unit y length. Two boundary conditions on Eq. (4) are obtained from the continuity of H across the junction edges. Using (2) we have

$$\begin{aligned} (\hbar c/2ed)(\partial\phi/\partial z)|_0 &= H(0), \\ (\hbar c/2ed)(\partial\phi/\partial z)|_L &= H(L). \end{aligned} \quad (6)$$

Now $H(0)$ and $H(L)$ are simply related by Ampere's Law to I and H_e .

$$\begin{aligned} H(L) - H(0) &= 4\pi I/c \\ &= \hbar c/2ed[\partial\phi/\partial z|_L - \partial\phi/\partial z|_0], \end{aligned} \quad (7)$$

$$\begin{aligned} H(L) + H(0) &= 2H_e \\ &= \hbar c/2ed[\partial\phi/\partial z|_L + \partial\phi/\partial z|_0]. \end{aligned} \quad (8)$$

The last equalities follow from Eq. (6) and relate the end-point gradients of the phase to I and H_e .⁶

Equation (4) can be put into a standard elliptic integral form by integrating to get

$$\partial\phi/\partial z = \lambda_J^{-1} [2(C - \cos\phi)]^{1/2}. \quad (9)$$

Then setting $C = (2 - k^2)/k^2$, one obtains

$$\frac{z - z_0}{k\lambda_J} = \int_0^{\frac{1}{2}\phi - \frac{1}{2}\pi} \frac{d\theta}{[1 - k^2 \sin^2\theta]^{1/2}}, \quad (10)$$

which has as its solutions the Jacobian elliptic functions.

Assuming for a moment that $k \leq 1$, then ϕ is related to z by

$$\sin \frac{1}{2}\phi = \text{cn} \left(\frac{z - z_0}{k\lambda_J} \middle| k^2 \right), \quad (11a)$$

$$\cos \frac{1}{2}\phi = -\text{sn} \left(\frac{z - z_0}{k\lambda_J} \middle| k^2 \right). \quad (11b)$$

⁶ These are similar to equations obtained by Ivanchenko *et al.*, Ref. 5.

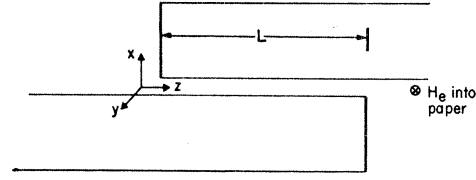


FIG. 1. The tunnel junction geometry assumed. The junction length is L and the applied H field is into the plane of the page.

Using the properties of the Jacobian elliptic functions, the magnetic field and current density can be written in the form

$$\begin{aligned} (2ed/\hbar c)H(z) &= \partial\phi/\partial z \\ &= \frac{2}{k\lambda_J} \text{dn} \left(\frac{z - z_0}{k\lambda_J} \middle| k^2 \right), \end{aligned} \quad (12a)$$

$$\begin{aligned} j(z) &= j_1 \sin\phi \\ &= -2j_1 \text{sn} \left(\frac{z - z_0}{k\lambda_J} \middle| k^2 \right) \text{cn} \left(\frac{z - z_0}{k\lambda_J} \middle| k^2 \right). \end{aligned} \quad (12b)$$

Here the sn, cn, and dn are Jacobian elliptic functions of argument $(z - z_0)/k\lambda_J$ and parameter k^2 . Using Eq. (7), the boundary conditions which determine the integration constants k^2 and z_0 are

$$\text{dn} \left(\frac{L - z_0}{k\lambda_J} \middle| k^2 \right) + \text{dn} \left(\frac{-z_0}{k\lambda_J} \middle| k^2 \right) = \frac{2ed}{\hbar c} k\lambda_J H_e, \quad (13a)$$

$$\text{dn} \left(\frac{L - z_0}{k\lambda_J} \middle| k^2 \right) - \text{dn} \left(\frac{-z_0}{k\lambda_J} \middle| k^2 \right) = \frac{4\pi ed}{\hbar c^2} k\lambda_J I. \quad (13b)$$

If $k \geq 1$, the equations for the field and current density become

$$\begin{aligned} (2ed/\hbar c)H(z) &= \partial\phi/\partial z \\ &= (2/k\lambda_J) \text{cn} \left(\frac{z - z_0}{\lambda_J} \middle| 1/k^2 \right), \end{aligned} \quad (14a)$$

$$j(z) = -(2j_1/k) \text{sn} \left(\frac{z - z_0}{\lambda_J} \middle| 1/k^2 \right) \text{dn} \left(\frac{z - z_0}{\lambda_J} \middle| 1/k^2 \right), \quad (14b)$$

and the boundary conditions are

$$\text{cn} \left(\frac{L - z_0}{\lambda_J} \middle| 1/k^2 \right) + \text{cn} \left(\frac{-z_0}{\lambda_J} \middle| 1/k^2 \right) = (2ed/\hbar c) k\lambda_J H_e, \quad (15a)$$

$$\text{cn} \left(\frac{L - z_0}{\lambda_J} \middle| 1/k^2 \right) - \text{cn} \left(\frac{-z_0}{\lambda_J} \middle| 1/k^2 \right) = (4\pi ed/\hbar c^2) k\lambda_J I. \quad (15b)$$

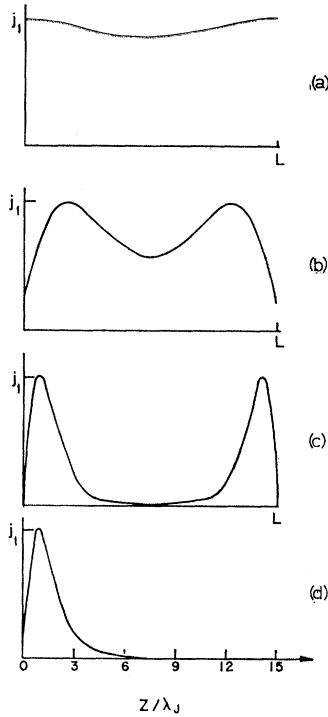


FIG. 2. Tunnel current density $j(z)$ in the junction when $I=I_{\max}$ and $H_e=0$ for: (a) $L=2\lambda_J$, (b) $L=5\lambda_J$, (c) $L=15\lambda_J$, and (d) $L=\infty$.

In principle, Eqs. (13) or (15) can be used to determine the parameters k and z_0 for given values of H_e and I . Then $j(z)$ is given by (12b) or (14b). However, since our goal was to find the maximum current that the junction could carry in a given magnetic field, the current was maximized subject to the boundary conditions. This was done by a graphical approach using tables and plots of the three Jacobian elliptic functions which appear in the equations.

The general method employed was to fix H_e and then determine the allowed values of k consistent with this H_e . For each choice of k we find the corresponding z_0 from Eq. (13a) or (15a). Finally, using k and z_0 , a value for I is obtained. Taking all k that are possible for solutions having a given H_e , we look for a maximum in the corresponding I values. For some ranges of H_e we find two or more relative current maxima. When this occurs, they are found to exist for different values of k which correspond to solutions with different numbers of whole vortices in the junction.

The parameter k has physical significance stemming from the fact that both the wavelength and the detailed shape of the current distribution depend on k . In the limit of small k , the current distribution has the familiar sinusoidal shape with a wavelength $\pi k\lambda_J$. As k increases, this sinusoidal shape becomes distorted and the period is given by $2k\lambda_J K(k^2)$. Here K is the com-

plete elliptic integral

$$K(k^2) = \int_0^{\pi/2} \frac{d\theta}{[1 - k^2 \sin^2\theta]^{1/2}}. \quad (16)$$

When the junction contains an integral number of wavelengths, i.e.,

$$L = n2k\lambda_J K(k^2), \quad (17)$$

the current distribution goes through n complete cycles between $z=0$ and $z=L$. Under these conditions the junction is said to contain n current vortices, and the total current I carried by the junction vanishes.

From Eq. (17) it follows that k decreases as the number of vortices in the junction increases. Since the shape of the elliptic functions depends upon k , the shape as well as the dimension of a vortex changes with the number of vortices in the junction. In Sec. III, Fig. 5(d) shows a solution in which the junction contains one vortex. The shape of this current distribution should be compared with the nearly sinusoidal current pattern shown in Fig. 7(d) for the case of three vortices.

III. RESULTS OF THE CALCULATION

In this section, the results obtained by solving the boundary-value problem given in Sec. II are discussed. It seems simplest to begin by discussing the current density for maximum current with zero external magnetic field. In the limit where the junction length is small compared to the Josephson penetration length, the current density is uniform. Figure 2(a) shows that the current density has only a slight deviation from uniformity for $L/\lambda_J=2$. However, as L/λ_J increases further [see Figs. 2(b) and 2(c)], the current density decreases in the center and peaks near the edges. This is simply the Meissner effect for our junction. Figure 2(d) gives a plot of the current density obtained by Ferrell and Prange in their analysis of a semi-infinite junction.⁴ It is clear that our results near the two edges of a long junction, Fig. 2(c), are consistent with the current density for a semi-infinite junction. According to the Landau-Ginzburg equations, the current density in a superconductor is proportional to the gradient of the pair phase. This implies that the current density is a maximum at the surface of a bulk supercon-

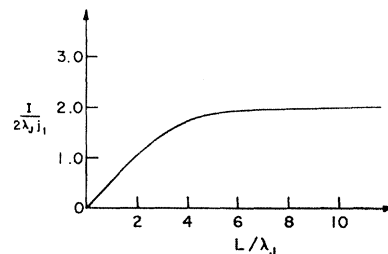


FIG. 3. Maximum total current versus junction length L for $H_e=0$.

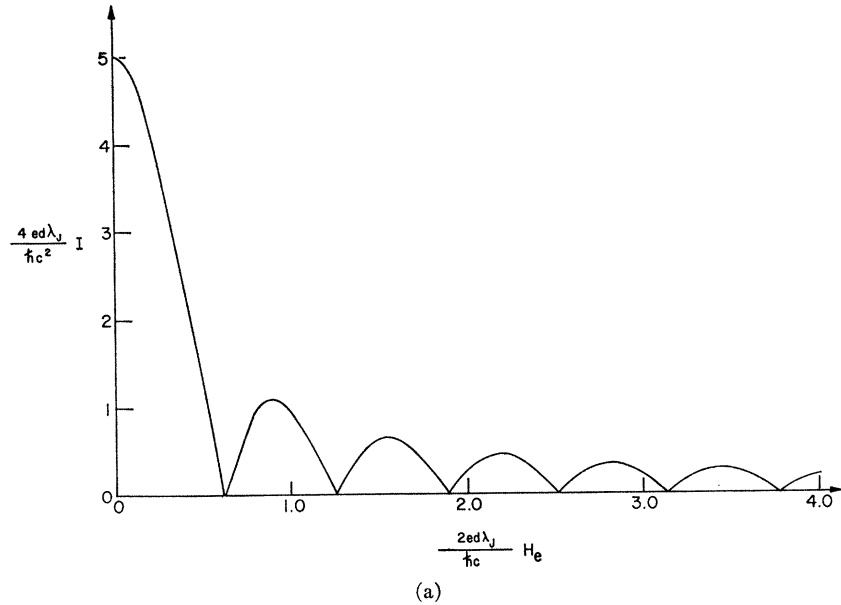
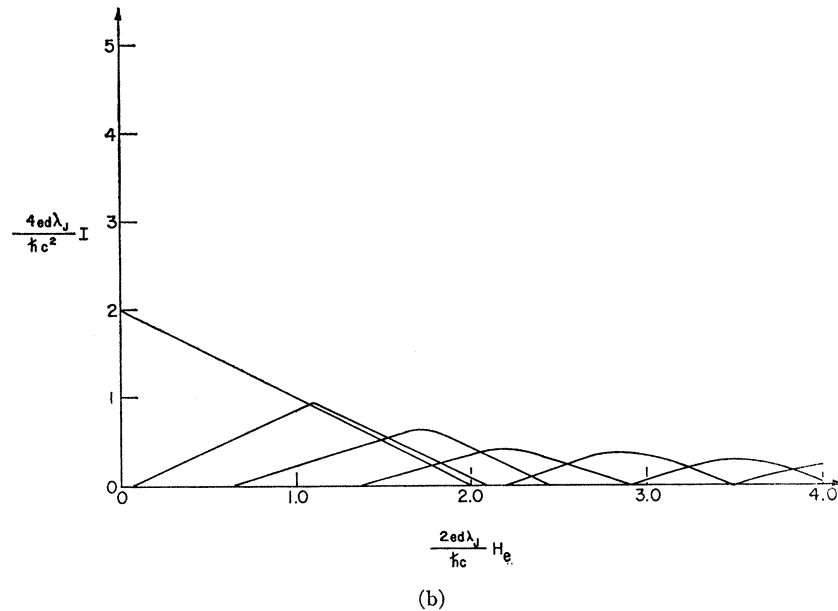


FIG. 4. (a) The Fraunhofer pattern approximation for the critical current versus applied field when $L=10\lambda_J$. (b) Results of the calculation using Jacobian elliptic functions when $L=10\lambda_J$. Note the striking dissimilarity for this large L/λ_J ratio.



ductor. However, in the case of a superconducting tunnel junction, the current density is proportional to the sine of the phase difference φ across the junction. Like the phase gradient in the bulk superconductor, this phase difference decreases with depth into the sample. If the current were proportional to φ divided by the junction barrier thickness (analogous to the bulk superconductor), the current density would be maximum at the edge. However, since the current density is proportional to $\sin \varphi$, the peak will occur where φ has dropped to $\pi/2 \pmod{2\pi}$. Under the maximum current conditions shown in Figs. 2(c) and 2(d), the phase drops from $\pi \pmod{2\pi}$ at the edge, giving zero

current density at the edge and peak current at a distance of order λ_J into the junction.

In Fig. 3 the total current for zero external magnetic field is plotted as a function of the junction length. Initially the maximum current carrying capacity per unit width increases linearly with L , reflecting the uniformity of the current density. However, for L greater than $4\lambda_J$, the current rapidly saturates at the value $4\lambda_J j_1$. An amount of current $2\lambda_J j_1$, is carried on each edge as originally discussed in Ref. 4.

In the presence of an external magnetic field, the current density changes. For a junction having a small L/λ_J ratio, the current density which maximizes

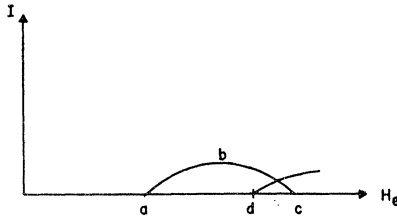


FIG. 5. The general shape of I_{crit} as a function of applied magnetic field for a mode containing between n and $n+1$ vortices.

the current is

$$j(z) = j_1 \cos \left[(2ed/\hbar c) H_e (z - L/2) \right]. \quad (18)$$

The current versus magnetic field follows a Fraunhofer diffraction pattern⁵

$$I = j_1 L \left| \frac{\sin \left[(ed/\hbar c) H_e L \right]}{(ed/\hbar c) H_e L} \right|. \quad (19)$$

For a large L/λ_J ratio the behavior is quite different. In Fig. 4, the critical current (solid line) is plotted as a function of magnetic field for a junction with an L/λ_J ratio of 10. As the magnetic field H_e increases from zero, we find that the total current initially decreases linearly with H_e according to the equation

$$I = 4\lambda_J j_1 - (c/4\pi) H_e. \quad (20)$$

This result can be understood as follows. As we have seen, in a long junction in zero field the current density is essentially restricted to the ends. Let us call I_l the current flowing on the left-hand edge and I_r the current on the right-hand edge. In the presence of a small magnetic field, the currents carried at the ends differ by an amount

$$I_r - I_l = (c/2\pi) H_e \quad (21)$$

necessary to shield the external field from the junction center. Since the maximum current at an edge cannot exceed $2\lambda_J j_1$, the critical junction current is obtained when $I_r = 2\lambda_J j_1$. Combining this with Eq. (21), the critical current $I_l + I_r$ is given by (20). At the bottom of the linear portion, $I_l = -I_r$ and the net tunneling current $I = 0$. Here the junction contains exactly one whole current vortex consisting of tunneling current in the $+x$ direction at the right end and in the $-x$ direction on the left.

In order to discuss the rest of Fig. 4, we find it convenient to categorize solutions by the number of complete vortices present in the junction. Solutions where in the junction contains more than n but less than $n+1$ vortices we call the " n to $n+1$ vortex mode" for the junction. We find that solutions in a given mode can exist for only a finite range of H_e . Furthermore,

for some ranges of H_e , it is possible for the junction current density to vary in the sense that several modes characterized by different vortex numbers and different critical currents can exist at a given H_e . A plot of the maximum I versus H_e for the n to $n+1$ mode will look like the curve abc in Fig. 5. At point a the junction contains exactly n vortices and at point c exactly $n+1$. The maximum-current-versus- H_e curve for the $n+1$ to $n+2$ mode is similar in shape. However, as shown in Fig. 5, it starts at point d and overlaps part of the n to $n+1$ mode. This leads to the structure shown in Fig. 4 for a junction of length $L = 10\lambda_J$.

Physically, the overlap is a consequence of the fact that the spatial variation of the phase ϕ is determined by the *total* magnetic field at each point in the junction. This includes both the externally applied field and the field produced by the junction currents. The result is that for a given H_e solutions may be possible having different values for the period and shape of the vortex structure and also for the junction current I . Between points d and c , the allowed solutions include possibilities having both less than and more than $n+1$ vortices, that is to say, solutions in both the n to $n+1$ mode and in the $n+1$ to $n+2$ mode. Calculations of the maximum current possible for solutions in the n to $n+1$ mode gives a curve that falls to zero as H_e approaches point c . The maximum I for solutions in the $n+1$ to $n+2$ mode rises from zero as H_e increases from point d . One result of the overlapping discussed above is that for every $H_e > 0$ we can find some mode of operation for the junction which allows a total current $I > 0$. This has been observed experimentally⁷ and is in contrast with the Fraunhofer pattern seen for short junctions where periodically $I_{\text{max}} = 0$.

In addition to the behavior of the critical current as a function of the applied magnetic field, our solutions give us details concerning the current density $j(z)$. This tells us the actual shape of the vortices. First, however, we consider the situation where the junction contains less than one whole vortex. For long junctions the maximum I that can be carried by the junction in this mode depends on H_e in the linear manner discussed previously. In Fig. 6 we have arbitrarily chosen four values of H_e and taken $L = 10\lambda_J$. Using the solution in the 0 to 1 vortex mode which has the maximum I for each H_e chosen, we have graphed the current density and magnetic field in the junction for each of these four cases. Note that when the reduced field $\mathcal{H} = (2ed/\hbar c \lambda_J H_e) = 2$, the only solution possible in the 0 to 1 vortex mode is the one-vortex solution. This solution carries zero net current I and is the solution at the bottom of the linear portion of the I_{max} -versus- H_e graph seen in Fig. 4.

⁷ Measurements of I_c versus H have been carried out by A. Goldman (to be published). The results are in good agreement with the behavior we have discussed.

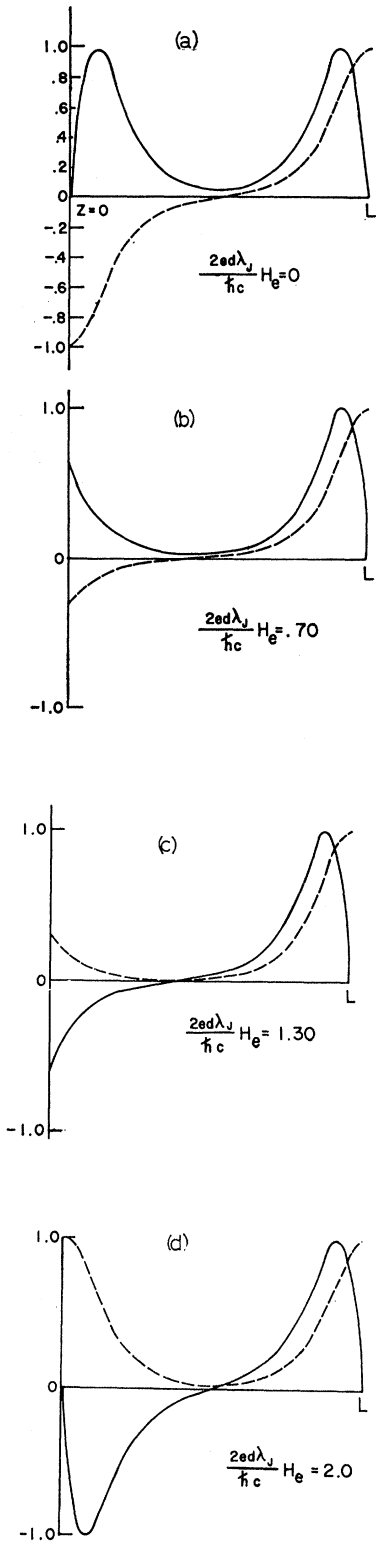


FIG. 6. The current density and the local magnetic field within the junction for four solutions in the 0 to 1 vortex mode. The solid line is $j(z)/j_1$; the broken line is $(2ed/\hbar c)\lambda_J H(z)$. The horizontal axis runs from $z=0$ to $z=L=10\lambda_J$.

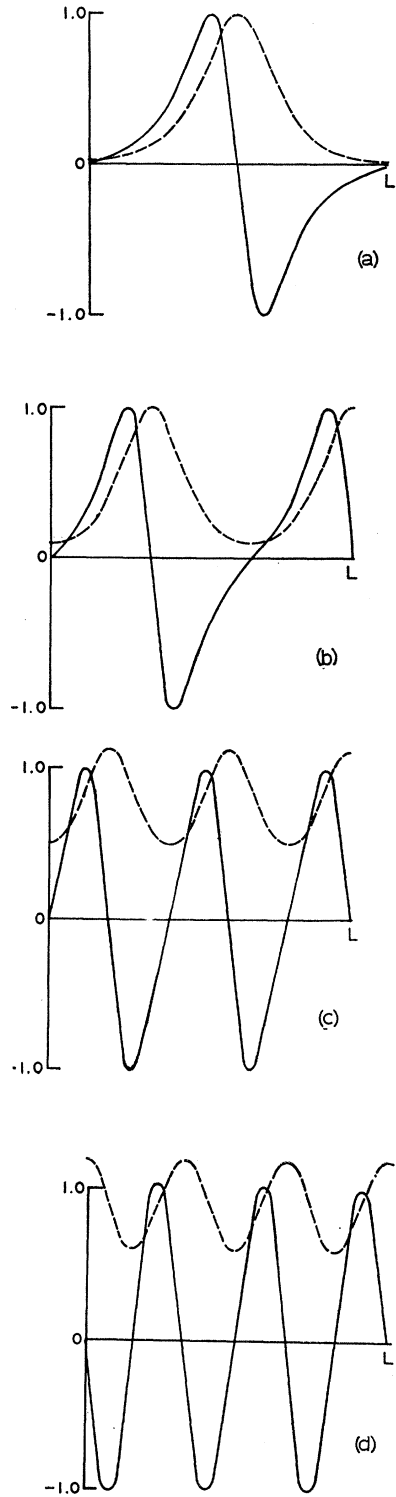


FIG. 7. Current density $j(z)/j_1$ (solid line) and magnetic field $(2ed/\hbar c)\lambda_J H(z)$ (broken line) for $L=10\lambda_J$: (a) at $\mathcal{I}C = (2ed\lambda_J/\hbar c)$, $H_e=0.06$, the one-vortex solution at its lowest possible $\mathcal{I}C$, (b) at $\mathcal{I}C=1.08$ when I_c is at its maximum for the 1-2 mode of solution, (c) at $\mathcal{I}C=1.72$ when I_c is greatest for the 2-3 mode, (d) at $\mathcal{I}C=2.44$, the three-vortex solution at its greatest possible $\mathcal{I}C$.

We have already noted that different solutions containing n vortices will occur at different H_e depending on whether they are part of the $n-1$ to n vortex mode or the n to $n+1$ mode. The current density and magnetic field plots for the two cases will look different even though both solutions fit exactly n vortices into the junction. Figure 6(d) can be compared with Fig. 7(a), which also shows a one-vortex solution but at $\beta C = 0.06$. This solution is the start of the 1 to 2 vortex mode.

Solutions with a nonintegral number of vortices in the junction are also possible. In fact, since a complete vortex does not contribute to the total current I , all solutions with $I > 0$ are of this type. A solution in the 1 to 2 vortex mode is shown in Fig. 7(b). A solution in the 2 to 3 vortex mode is shown in Fig. 7(c). We can see that as more vortices fit into the junction they not only have a smaller dimension, but they become more sinusoidal in shape as well. The magnetic field $H(z)$ is smoothing out as H_e is increased, since the modulating action of the tunneling currents has less effect on larger applied fields.

IV. CONCLUSIONS

The emphasis in this work has been to obtain the details of the current-magnetic-field behavior of a superconducting tunnel junction. Such junctions exhibit the phenomena of vortex structure in a particularly simple and direct way. From a theoretical point of view, exact solutions are available. From an experimental point of view, the details of the vortex structure can be probed by simply measuring the current-field behavior.⁷

In this paper we have dealt with the static properties of the vortex structure. A similar detailed analysis of the dynamics of the transition between different vortex modes would be of interest. It would provide a simple model for vortex creation phenomena. Experimentally, we expect that the dynamics of the creation process are reflected in the anomalous continuous voltage-magnetic-field structure observed in tunnel junctions with large L/λ_J ratios.⁸ The dynamics of the transition between different vortex modes could also be investigated.

⁸ D. N. Langenberg, D. J. Scalapino, B. W. Taylor, and R. E. Eck, *Phys. Letters* **20**, 563 (1966).

Meissner Effect and Vortex Penetration in Josephson Junctions*

A. M. GOLDMAN† AND P. J. KREISMAN‡

School of Physics and Astronomy, University of Minnesota, Minneapolis, Minnesota

(Received 29 May 1967)

Investigation of the magnetic field dependence of the maximum zero-voltage current of wide, high-current Josephson junctions has revealed behavior drastically different from the usual Fraunhofer pattern for narrow junctions. The experiments are interpreted as evidence for a Meissner effect for the insulating layer and adjacent penetration layers of wide junctions in low external fields, and for an eventual transition to a mixed state as the external field is increased from zero.

I. INTRODUCTION

THE most striking experimental evidence for the existence of the Josephson effect is the magnetic field dependence of the maximum zero-voltage tunneling current of narrow, weakly-coupled Josephson junctions. In a narrow junction, the dimension L of the junction perpendicular to the field is much smaller than the Josephson penetration depth λ_J .¹ We have been in-

vestigating the field dependence of the maximum zero-voltage tunneling current of wide ($L \gg \lambda_J$) high current junctions, and have observed behavior different from the Fraunhofer^{2,3} pattern obtained for narrow junctions. From the measurements, it is possible to infer that wide junctions exhibit a Meissner effect at low external fields and an eventual transition to a mixed state as the external field is increased. The experiments indirectly probe field and current distributions in the insulating layer and adjacent penetration layers of the junctions. Some of the features of the observed behavior, which is a consequence of the "self"-fields generated by the tunneling currents, have already been

* Work supported by the U.S. Atomic Energy Commission under contract AT-(11-1)1569 by the Graduate School of the University of Minnesota, and by the Alfred P. Sloan Foundation.
† Alfred P. Sloan Foundation Fellow.

‡ National Aeronautics and Space Administration trainee.

¹ The quantity $\lambda_J = [\hbar c^2 / 8\pi e J_1 d]^{1/2}$ is the Josephson penetration depth. In the expression $d = 2\lambda_L + t$, J_1 is the maximum Josephson current density, c is the velocity of light, e is the electronic charge, λ_L is the London penetration depth, and t is the oxide layer thickness.

² J. M. Rowell, *Phys. Rev. Letters* **11**, 200 (1963).

³ M. D. Fiske and I. Giaever, *Proc. IEEE* **52**, 1155 (1964).